

Human Enteroid Monolayers: A Novel, Functionally-Stable Model for Investigating Oral Drug Disposition

Christopher Arian¹, Eimear O'Mahony¹, James W. MacDonald², Theo K. Bammler², Mark
Donowitz³, Edward J. Kelly^{1,4} and Kenneth E. Thummel¹

¹Department of Pharmaceutics, School of Pharmacy, University of Washington, Seattle WA

²Department of Environmental and Occupational Health Sciences, School of Public Health,
University of Washington, Seattle WA

³Department of Medicine, Division of Gastroenterology and Department of Physiology, School
of Medicine, Johns Hopkins University, Baltimore, MD

⁴Kidney Research Institute, University of Washington, Seattle, WA

Corresponding Authors:

Names: Edward J. Kelly & Kenneth E. Thummel

Address: University of Washington School of Pharmacy
Department of Pharmaceutics
H-272 Health Sciences Building, Box 357610
Seattle, Washington 98195

Emails: edkelly@uw.edu , thummel@uw.edu

Phones: 206-685-4641 , 206-543-0819

Fax: 206-543-3204

TABLE OF CONTENTS

1. **Running Title Page** – Page 4
2. **Abbreviations** – Page 5
3. **Abstract** – Page 6
4. **Significance Statement** – Page 7
5. **Introduction** – Page 8-10
6. **Materials and Methods** – Page 10-25
7. **Results** – Page 25-28
8. **Discussion** – Page 28-33
9. **Acknowledgements** – Page 34
10. **Author Contributions** – Page 35
11. **References** – Page 36-38
12. **Footnotes** – Page 39
13. **Tables** – Page 40
14. **Figure Legends** – Page 41-43

RUNNING TITLE PAGE

Running Title: Human Enteroid Monolayers: A Novel, Functionally-Stable Model
for Investigating Oral Drug Disposition

Number of text pages: 37

Number of tables: 1

Number of figures: 6

Number of words in:

Abstract: 225

Introduction: 714

Discussion: 1502

Number of references: 23

Abbreviations

2D, 2-dimensional; 3D, 3-dimensional; ABC, ATP-binding cassette; BCS, biopharmaceutical classification system; CBC, crypt-base columnar cell; DMEM/F-12, Dulbecco's Modified Eagle Medium; DMET, drug metabolizing enzymes and transporters; DPBS⁺⁺, Dulbecco's phosphate-buffered saline with calcium and magnesium; HBSS⁺⁺, Hank's balanced salt solution with calcium and magnesium; HSA, human serum albumin; ICC, immunocytochemistry; LGR5, Leucine-rich repeat-containing G-protein coupled receptor 5; MBI, mechanism-based inhibitor; MKI67, marker of proliferation Ki-67; MRP3, Multidrug Resistance associated Protein 3; MUC2, mucin 2; NME, new molecular entity; PCNA, proliferating-cell nuclear antigen; SLC, solute carrier; TEER, transepithelial electrical resistance; UPLC, ultra-performance liquid chromatography; VDR, vitamin D receptor; ZO-1, zonula occludens-1; ZO-3, zonula occludens-3.

ABSTRACT

To further the development of an *in vitro* model which faithfully recapitulates drug disposition of orally administered drugs, we investigated the utility of human enteroid monolayers to simultaneously assess intestinal drug absorption and first-pass metabolism processes. We cultured human enteroid monolayers from three donors, derived via biopsies containing duodenal stem cells that were propagated and then differentiated atop permeable Transwell® inserts, and confirmed transformation into a largely enterocyte population via RNA-seq analysis and immunocytochemical (ICC) assays. Proper cell morphology was assessed and confirmed via bright field microscopy and ICC imaging of tight junction proteins and other apically and basolaterally localized proteins. Enteroid monolayer barrier integrity was demonstrated by elevated transepithelial electrical resistance (TEER) that stabilized after 10 days in culture and persisted for 42 days. These results were corroborated by low paracellular transport probe permeability at 7 and 21 days in culture. The activity of a prominent drug metabolizing enzyme, CYP3A, was confirmed at 7, 21, and 42 days culture under basal, $1\alpha,25(\text{OH})_2$ vitamin D₃-induced, and 6',7'-dihydroxybergamottin-inhibited conditions. The duration of these experiments is particularly noteworthy, as this is the first study assessing drug metabolizing enzymes and transporters (DMET) expression/function for enteroids cultured for greater than 12 days. The sum of these results suggests enteroid monolayers are a promising *ex vivo* model to investigate and quantitatively predict an orally administered drug's intestinal absorption and/or metabolism.

SIGNIFICANCE STATEMENT

This study presents a novel *ex vivo* model of the human intestine, human intestinal organoid (enteroid) monolayers, that maintain barrier function and metabolic functionality for up to 42-days in culture. The incorporation of both barrier integrity and metabolic function over an extended period within the same model is an advancement over historically used *in vitro* systems, which either lack one or both of these attributes or have limited viability.

INTRODUCTION

Oral administration of pharmaceutical compounds is the most common and popular route of drug administration. After dissolution in the gastric fluid, the first barrier an orally administered drug must face before it can reach systemic blood circulation is primarily the intestinal mucosa, though some absorption can occur *via* the stomach, depending on the compound. Following absorption across an apical membrane of villus enterocytes, drug can be transformed by phase I and/or phase II metabolic reactions or transported unchanged across the basolateral enterocyte membrane, gaining access to the splanchnic capillaries that feed the portal vein and liver. Paracellular transport between enterocytes is an alternative, but less efficient route of absorption, depositing drug into the same capillaries and into vena cava blood via the lymphatic system. Parent drug delivered to the liver is subject to another round of metabolic elimination and/or biliary excretion. That which remains intact after navigating the intestinal and hepatic barriers will reach the systemic blood circulation, where it can then be delivered to its site of action (Rowland et al., 2009). Thus, intestinal drug disposition can profoundly affect pharmacological response following oral drug administration.

Drug elimination in the intestine and liver are termed the “first-pass effect” and contribute to an orally dosed drug’s bioavailability (F), which can be mathematically described by the equation:

$$F = F_A * F_G * F_H$$

where F_A is the net fraction of drug that is absorbed by the intestine, F_G is the fraction of drug that escapes metabolism in the intestine, and F_H is the fraction of drug that escapes hepatic metabolism/biliary excretion. Characterizing intestinal drug absorption efficiency and first-pass

elimination of a new molecular entities (NMEs) is a key step in the drug development pathway, often predicted pre-clinically with the use of *in vitro* models of human intestinal and hepatic functions. Strikingly, historically used *in vitro* models of the human intestine all have limitations which hinder broad and accurate predictions of the F_A and F_G components of oral bioavailability (Arian et al., 2022). The shortcomings of these models underscore the need for a more complete *in vitro* model that can fully recapitulate drug absorption and metabolism processes that occur *in vivo*. A promising complex *ex vivo* system of the human intestine that can potentially fill this research need are adult intestinal stem cell-derived organoids, or enteroids, which are multicellular, 3-dimensional structures that recapitulate intestinal functions under appropriate culture conditions (Rossi et al., 2018).

The adult intestinal stem cells, or $LGR5^+$ crypt-base columnar cells (CBCs), are isolated and cultured within a Matrigel droplet in culture medium containing the key growth factors, Wnt3A, R-spondin-1, and Noggin. This high growth factor medium is necessary for the formation of 3-dimensional (3D) intestinal spheroids, which are undifferentiated enteroids (i.e., contain mostly $LGR5^+$ CBC and Paneth cells). Removal of the aforementioned growth factors, most notably Wnt3A, will cause the 3D intestinal spheroids to differentiate in the Matrigel plugs, giving rise to 3D differentiated enteroids (Sato et al., 2011). Due to the inside out nature of 3D enteroids (i.e., apical membrane is localized to the inside of the enteroids), the apical membrane can only be accessed via microinjecting the organoids or by flipping the membrane by treating with a chelating agent (e.g., EGTA) after Matrigel removal to mimic oral drug administration to the luminal membrane of the intestinal epithelium. However, culturing protocols have been developed which dissociate the 3D undifferentiated intestinal spheroids so they can be plated as 2-dimensional (2D) monolayers atop Transwell® filters, and when growth factors are removed,

monolayer differentiation can be achieved (Foulke-Abel et al., 2016; In et al., 2016). Complete removal of Wnt3A results in terminal differentiation, providing 5-12 days of viability before substantial cell death and loss of drug metabolizing enzyme and transporter (DMET) activity occurs. Using this protocol, groups have demonstrated robust activity of several highly expressed intestinal DMETs such as CYP3A4, CYP2C9, UGT1As, CES2, and P-glycoprotein (P-gp, ABCB1) (Vermetti et al., 2017; Kasendra et al., 2020; Michiba et al., 2022). While these results are exciting, the relatively short and dynamic culture period of roughly one week limits this model from use in protracted investigations, such as long-term toxicology studies, mechanism-based inactivator (MBI) studies, and induction/deinduction time course studies.

In our hands, duodenal enteroid monolayers differentiated using a proprietary medium which supports differentiation resulted in culture viability of at least 42 days. We used immunocytochemical (ICC) imaging, mRNA analysis, TEER measurements, and selective CYP3A probe disposition to confirm cell differentiation, characterize monolayer barrier function, and confirm CYP3A metabolic activity during the entire period.

MATERIALS AND METHODS

Chemicals and reagents. IntestiCult™ Organoid Growth Medium (Human), IntestiCult™ Organoid Differentiation Medium (Human), and Y-27632 (Dihydrochloride) were purchased from STEMCELL Technologies (Vancouver, BC, Canada). Advanced DMEM/F-12, DMEM, MEM, fetal bovine serum (FBS), Trypsin-EDTA (0.25%), Versene solution, Penicillin-Streptomycin (10,000 U/mL), Dulbecco's phosphate-buffered saline with calcium and magnesium (DPBS⁺⁺), DPBS without calcium and magnesium, HEPES buffer (1M), Hanks' Balanced Salt Solution with calcium and magnesium (HBSS⁺⁺), Tween-20, dextran 70, SlowFade™ Diamond Antifade mountant with DAPI, and ProLong™ Gold antifade reagent

were purchased from Life Technologies (Carlsbad, CA). Gelatin-based coating solution (0.1%) and Complete Epithelial cell medium kit were purchased from Cell Biologics (Chicago IL). Midazolam, midazolam-d₄, 1-OH midazolam, and 1-OH midazolam-d₄ were purchased from Cerilliant (Round Rock, TX). Matrigel® Growth Factor Reduced (GFR) Basement Membrane Matrix (phenol red-free, LDEV-free), collagen IV, and Cell Recovery Solution were purchased from Corning (Corning, NY). Atenolol-d₇, digoxin-d₃, and 6',7'-dihydroxybergamottin were purchased from Cayman Chemical (Ann Arbor MI). Atenolol, digoxin, verapamil hydrochloride, rifampin, triton X-100, and sodium bicarbonate were purchased from Sigma-Aldrich (St. Louis, MO). RLT Lysis buffer was purchased from Qiagen (Germantown, MD). Normal goat serum (2.5%) was purchased from Vector Laboratories (Newark, CA). Human serum albumin (low endotoxin) was purchased from Gemini Bio (West Sacramento, CA). Paraformaldehyde (16%) was purchased from Electron Microscopy Sciences (Hatfield, PA). 1 α ,25(OH)₂ vitamin D₃ was purchased from Calbiochem (La Jolla, CA). Rabbit monoclonal antibody to Villin (ab130751), rabbit monoclonal antibody to Ki67 (ab16667), mouse monoclonal antibody to Occludin (ab242202), rabbit polyclonal antibody to MRP3 (ab204322), rabbit monoclonal antibody to Zonula Occludens protein 3 (ab181991), rabbit monoclonal antibody to ZO1 tight junction protein (ab221547), Alexa Fluor 647 goat polyclonal antibody to mouse IgG (ab150115), Alexa Fluor 488 goat polyclonal antibody to rabbit IgG (ab150077), and Alexa Fluor 647 goat polyclonal antibody to rabbit IgG (ab150079) were purchased from Abcam (Cambridge, UK).

Cell culture. Anonymized undifferentiated duodenal organoids from three donors (27 year old, female; 81 year old, female; 25 year old, male) derived *via* endoscopy for clinically indicated conditions, where upper GI tract was endoscopically normal, were kindly provided by Dr. Mark Donowitz, Johns Hopkins University, MD. The original biopsy samples were collected in

accordance with the Institutional Review Board of John's Hopkins University (protocol numbers IRB-NA_00038329 and IRB-00044373). Experiments were conducted at passages 28 – 38. Undifferentiated organoids were suspended and grown in Matrigel droplets in the presence of Intesticult™ Intestinal Organoid Growth Medium (Human) containing 1% (v/v) penicillin-streptomycin. Undifferentiated organoids were passaged after 7-10 days in culture, or until they reached a large, cystic morphology, by the addition of 0.5 mL of cold Cell Recovery Solution followed by 30 minutes of shaking at 4°C. Cells were then triturated until roughly 80% of the organoids were broken into small fragments followed by centrifugation for 10 minutes at 1200g at 4°C. The resulting supernatant was discarded and the cell pellet was resuspended with Matrigel and plated onto a 24-well plate in 50 µL droplets. The plate was then placed into a 37°C incubator for 10-15 minutes to allow for the Matrigel to polymerize, followed by the addition of 0.5 mL of Intesticult™ Growth Medium containing 10 µM Y-27632. Undifferentiated organoids were fed every two days with Intesticult™ Growth Medium without Y-27632. Cells were split from 1:2 to 1:5, depending on cell density.

Enteroid monolayers were grown on polyester, 0.4 µm pore-size Transwell® filter inserts for 24-well plates (catalog no. 3470; Corning Inc., NY). The day before seeding, 50 µL of 34 µg/mL collagen IV was added to each Transwell® and allowed to polymerize overnight in a 37°C incubator. The following day, undifferentiated organoids were removed from their Matrigel droplets (two Matrigel droplets per Transwell® insert plated) by the addition of 0.5 mL of cold Cell Recovery Solution followed by 30 minutes of shaking at 4°C. Cells were then triturated on ice until roughly 95% of the organoids were broken into small fragments/single cells followed by centrifugation for 10 minutes at 1200g at 4°C. The resulting supernatant was discarded and the cell pellet was resuspended with Intesticult™ Intestinal Organoid Differentiation Medium

(Human) containing 1% (v/v) penicillin-streptomycin and 10 μ M Y-27632. Buffer in the collagen IV-treated Transwell® inserts was then aspirated and the inserts washed with Advanced DMEM/F-12 before plating 100 μ L of the cell suspension to each Transwell® insert (apical chamber) and addition of 0.5 mL of the Intesticult™ Differentiation Medium to the basolateral chamber of the 24-well plate. Enteroid monolayers were fed every two days by aspirating apical and basolateral media and replacing with 0.1 mL and 0.5 mL of Intesticult™ Differentiation Medium containing Y-27632 to the apical and basolateral chambers, respectively. For undifferentiated monolayers, the cell pellet was resuspended with Intesticult™ Growth Medium containing Y-27632, plated, and then fed every two days by aspirating apical and basolateral media and replacing with 0.1 mL and 0.5 mL with growth medium containing Y-27632 to the apical and basolateral chambers, respectively.

Cryopreserved human primary small intestinal epithelial cells (catalog no. H-6051, Cell Biologics Inc, IL) from a single donor were cultured as described by the vendor. Briefly, cells were thawed then cultured for two days in a gelatin-coated T25 flask containing Complete Epithelial cell medium. After two days, cells were washed with warm DPBS (without calcium and magnesium) then incubated with 2 mL 0.25% trypsin-EDTA solution for 3-6 minutes at room temperature to detach cells followed by washing with Complete Epithelial cell medium to neutralize the trypsin. Cells were then centrifuged at 500g for 6 minutes at room temperature. Supernatant was then removed and the cell pellet was resuspended in Complete Epithelial cell medium at a density of 350,00 cells/mL. Cell slurry (0.25 mL) was plated on a gelatin-coated 0.4 μ m pore-size Transwell® filter inserts for 24-well plates (catalog no. 3470; Corning Inc., NY) and 1 mL of Complete Epithelial cell medium was added to the basolateral chamber. Cells were fed every two days by aspirating apical and basolateral medium and replacing with 0.25 mL and

1 mL of Complete Epithelial cell medium to the apical and basolateral chambers, respectively.

Cells were grown for 7 days prior to CYP3A activity assessment.

LS180 cells (passage 38) were cultured in a T75 flask with MEM supplemented with 10% (v/v) FBS and 1% (v/v) penicillin-streptomycin. After 7 days in culture, cells were washed with warm DPBS (without calcium and magnesium) then incubated with Versene 1x for 5 minutes at room temperature. Suspended cells were then centrifuged at 1200g for 2 minutes. The resulting cell pellet was resuspended in MEM containing 10% FBS and 1% penicillin-streptomycin at a density of 167,000 cells/mL as determined by a hemocytometer. 0.25 mL of the cell slurry was plated on a 0.4 μ m pore-size Transwell® filter inserts for 24-well plates (catalog no. 3470; Corning Inc., NY) that were coated with 34 μ g/mL collagen IV as described above. 1 mL of MEM containing 10% FBS and 1% penicillin-streptomycin was then added to the basolateral chamber. Cells were fed every two days by aspirating apical and basolateral medium and replacing with 0.25 mL and 1 mL of MEM containing 10% FBS and 1% penicillin-streptomycin to the apical and basolateral chambers, respectively. Cells were grown for 7 days prior to CYP3A activity assessment.

Caco-2 cells (passage 29) were cultured in a T75 flask with DMEM supplemented with 10% (v/v) fetal bovine serum (FBS) and 1% (v/v) penicillin-streptomycin. After 7 days in culture, cells were washed with warm DPBS (without calcium and magnesium) then incubated with 3 mL of 0.25% trypsin-EDTA solution for 5 minutes at 37°C for 5 minutes by washing with DMEM containing 10% FBS and 1% penicillin-streptomycin to neutralize the trypsin. Cells were then centrifuged at 1000g for 5 minutes at room temperature. Supernatant was then removed and the cell pellet was resuspended in DMEM containing 10% FBS and 1% penicillin-streptomycin at a density of 167,000 cells/mL as determined by a hemocytometer. 0.25 mL of the

cell slurry was plated on a 0.4 μm pore-size Transwell® filter inserts for 24-well plates (catalog no. 3470; Corning Inc., NY) that were coated with 34 $\mu\text{g}/\text{mL}$ collagen IV as described above. 1 mL of DMEM containing 10% FBS and 1% penicillin-streptomycin was then added to the basolateral chamber. Cells were fed every two days by aspirating apical and basolateral medium and replacing with 0.25 mL and 1 mL of DMEM containing 10% FBS and 1% penicillin-streptomycin to the apical and basolateral chambers, respectively. Cells were grown for 21 days prior to CYP3A activity assessment.

For enteroid monolayer induction and inhibition experiments, differentiation medium was removed and the cells were washed three times with DPBS⁺⁺ followed by addition of 0.1 mL and 0.5 mL of Intesticult™ Differentiation Medium containing compound or vehicle to the apical and basolateral chambers, respectively, for 48 hours. Stock solutions of $1\alpha,25(\text{OH})_2$ vitamin D₃ (1 μM in ethanol), 6',7'-dihydroxybergamottin (50 mM in DMSO), or rifampin (50 mM in DMSO) were prepared and diluted 1000-fold in Intesticult™ Differentiation Medium containing Y-27632.

RNA-seq analysis for undifferentiated and differentiated organoids. Matched undifferentiated spheroids and differentiated enteroid monolayers cultured for 21 days from the same donor at the same passage number were lysed with 0.5 mL of RLT lysis buffer (Qiagen Sciences Inc., Germantown, Maryland) and stored at -80°C until analysis. Samples were sent to Novogene America (Sacramento, California) where the RNA was isolated and messenger RNA was purified from total RNA using poly-T oligo-attached magnetic beads. mRNA was then fragmented and the first strand cDNA was synthesized using random hexamer primers, followed by second strand cDNA synthesis using dTTP for non-directional library and sequenced by a NovaSeq 6000 system (Illumina, San Diego, CA). Quality of the sequencing data was assessed

using fastqc (Andrews, 2010), and then reads were aligned to the Ensembl GRCh38 p12 genome using the HiSat2 aligner (Kim et al., 2019). Counts/gene were generated using the Bioconductor Rsubread (Liao et al., 2019) package. Total aligned reads ranged between 14.5M – 18M per sample. Pathway analysis of the RNA-seq data was performed using the iPathwayGuide software from ADVAITA (Advaita Corporation, Ann Arbor, MI). Genes with FDR <0.05 were used for pathway analysis. Details for the statistical analysis of the RNA-seq data are provided in the section further down titled “Statistical analysis”.

Immunocytochemistry and confocal microscopy. Enteroid monolayers grown on Transwell® inserts for 21 or 42 days were washed twice with DPBS⁺⁺, fixed in 4% formaldehyde in DPBS⁺⁺ for 15 minutes at room temperature, and then washed an additional three times with DPBS⁺⁺. Fixed monolayers were stored at 4°C for no more than 7 days. Monolayers stained for Villin and Ki-67 were permeabilized for 5 minutes at room temperature with DPBS⁺⁺ containing 0.1% Triton X-100. Permeabilized monolayers were then incubated in 0.05% Tween-20 and goat serum in DPBS⁺⁺ (blocking solution) for 60 minutes and subsequently incubated with a 100-fold dilution of primary antibody in blocking solution for 60 minutes. Monolayers were thereafter washed three times with DPBS⁺⁺ then incubated with a 1000-fold dilution of fluorescent-conjugated secondary antibody in blocking solution for 60 minutes. Monolayers were then washed an additional three times with DPBS⁺⁺.

After the fixing process, non-permeabilized monolayers (Occludin, MRP3, ZO-1, and ZO-3) were incubated with blocking solution for 60 minutes and subsequently incubated with a 100-fold dilution of primary antibody in blocking solution overnight at 4°C. Monolayers were thereafter washed three times with DPBS⁺⁺ then incubated with a 1000-fold dilution of

fluorescent-conjugated secondary antibody in blocking solution overnight at 4°C. The following day, monolayers were washed an additional five times with DPBS⁺⁺ while shaking.

Following the final washing step for both sets of monolayers, 50 µL of DAPI was added for 15 minutes and subsequently aspirated. Filters from each Transwell® insert were then cut out and mounted on glass microscope slides using ProLong Gold Antifade reagent. Images were captured and analyzed with a Nikon Eclipse Ti-S inverted microscope (Villin, Ki-67) using a 10x objective lens or with a Nikon A1R confocal microscope (Occludin, MRP3, ZO-1, and ZO-3) using a 40x oil immersion objective lens (Nikon, Melville, NY).

TEER measurement. Transepithelial electrical resistance was evaluated using an EVOM² epithelial voltohmmeter (World Precision Instruments, Sarasota, FL). Background resistance was determined for each set of cultures using a single Transwell® filter insert treated with collagen IV that was devoid of cells. The reported TEER values are a product of the background-corrected resistance and the surface area of the Transwell® insert.

Permeability assay. Cell monolayers were washed three times with blank apical transport buffer (10 mM HEPES in Hank's balanced salt solution, pH 6.5) and maintained at 37°C until use. Stock solutions of the test compounds (Midazolam, 3 mM in methanol; and atenolol, 60 mM in DMSO) were diluted in apical transport buffer to make their respective dosing solutions (final concentrations were 8 µM midazolam, 0.27% methanol; and 300 µM atenolol, 0.5% DMSO). Lucifer yellow dosing solution was made fresh for each assay by dissolving Lucifer yellow in apical transport buffer for a final concentration of 300 µM.

For the midazolam permeability measurement, 0.3 mL of the dosing solution was added to the filter insert and 0.7 mL of the receiver solution (10 mM HEPES in Hank's balanced salt solution,

pH 7.4, containing 0.27% methanol) was added to the basolateral compartment. Cells were incubated for 60 minutes at 37°C and the total volume from the apical and basolateral compartment were collected separately and stored at -80°C until analysis. Midazolam was quantified using liquid chromatography coupled with tandem mass spectrometry on an Agilent 6410 QQQ equipped with a UPLC 1290 system. After thawing and vortexing, 200 µL of basolateral sample and 50 µL of apical sample (diluted 4-fold in blank apical buffer to a final volume of 200 µL) was mixed with 250 µL of sodium carbonate buffer (100 mM, pH 11.4) and 20 µL of internal standard (midazolam-d₄, 150 ng/mL in methanol). A series of dilutions of midazolam standards were prepared in methanol and stored at -80°C. The standard curve was prepared using 10 µL of each stock solution and 200 µL of blank transport buffer and mixing with 250 µL of sodium carbonate buffer and 20 µL of internal standard. 3 mL of ethyl acetate was then added to the unknown and standard curve samples followed by 20 minutes of shaking and centrifugation at 2000g for 20 minutes at room temperature. The top organic layer was then collected and samples were dried using a nitrogen evaporator. Dried samples were then resuspended in 100 µL of 1:1 formic acid solution (0.1% in water): methanol and analyzed via LC/MS-MS. Chromatographic separation following injection of 5 µL sample was achieved using a Zorbax SB-C18 narrow-bore, 5 µm, 2.1 x 150 mm column using 0.1% formic acid in water (A) and methanol (B) as a mobile phase. The flow rate was 0.25 mL/min with a gradient as follows: 50% B for 1 minute, increased to 90% B linearly over 2 minutes, held at 90% for 3 minutes, and then equilibrated back to 50% for 4 minutes. The following MRM transitions were monitored: m/z 326.0 > 291.2 for midazolam, and m/z 330.0 > 295.0 for midazolam-d₄ in the positive ion mode. For both compounds, dwell time was set to 100 ms, fragmentor was set to 159V, collision energy was set to 28 eV, and cell accelerator voltage was set to 7V.

For the atenolol permeability measurement, 0.3 mL of the dosing solution was added to the filter insert and 0.7 mL of the receiver solution (10 mM HEPES in Hank's balanced salt solution, pH 7.4, containing 0.5% DMSO) was added to the basolateral compartment. Cells were incubated for 90 minutes at 37°C and the total volume from the apical and basolateral compartment were collected separately and stored at -80°C until analysis. Atenolol was quantified using liquid chromatography coupled with tandem mass spectrometry on an Agilent 6410 QQQ equipped with a UPLC 1290 system. After thawing and vortexing, 50 µL of basolateral samples and 50 µL of diluted apical samples (diluted 300-fold in blank apical transport buffer) were mixed with 20 µL internal standard (1.25 µM in methanol) and 30 µL of methanol. A series of dilutions of atenolol standards were prepared in methanol and stored at -80°C. The standard curve was prepared using 10 µL of each stock solution and 50 µL of blank transport buffer mixed with 20 µL of internal standard and 20 µL of methanol. Unknowns and standards were then centrifuged at 20,800g for 10 minutes at room temperature, and 75 µL of the supernatant was analyzed by LC/MS-MS. Chromatographic separation was achieved following injection of 5 µL of sample using a Zorbax SB-C18 narrow-bore, 5 µm, 2.1 x 150 mm column using 10 mM ammonium acetate (A) and methanol (B) as a mobile phase. The flow rate was 0.25 mL/min with a gradient as follows: 5% B for 1.5 minutes, then increased to 75% B linearly over 2 minutes, held at 75% for 4.5 minutes, and then equilibrated back to 5% for 4 minutes. The following MRM transitions were monitored: m/z 267.3 > 145.0 for atenolol, and m/z 274.3 > 145.2 for atenolol-d₇ in the positive ion mode. For both compounds, dwell time was set to 200 ms, collision energy was set to 29 eV, and cell accelerator voltage was set to 4 V. The fragmentor was set to 113 V for atenolol and 127 for atenolol-d₇.

For the Lucifer yellow permeability measurement, 0.3 mL of the dosing solution was added to the filter insert and 0.7 mL of the receiver solution (10 mM HEPES in Hank's balanced salt solution, pH 7.4) was added to the basolateral compartment. Cells were incubated for 60 minutes at 37°C and 300 µL of the basolateral compartment was collected. A series of dilutions of Lucifer yellow standards were prepared fresh during the 60-minute incubation period. The samples were analyzed by fluorescence detection using a Synergy HTX multi-mode reader (BioSPX, Netherlands) with excitation filter at 420 nm and emission filter at 528 nm.

Permeability coefficient calculation. The apparent cell monolayer permeability coefficient (P_{app} , cm/s) for midazolam was calculated using eq. 1 (Anoshchenko et al., 2021):

$$P_{app} = \frac{A_{MDZ,B}}{AUC_{MDZ,A} \cdot SA}$$

where $A_{MDZ,B}$ is the amount of unchanged midazolam (pmol) in the basolateral compartment under sink conditions (where less than 20% of the apically dosed midazolam was measured in the basolateral compartment), $AUC_{MDZ,A}$ is the area under the curve of unchanged midazolam concentration in the apical chamber versus time plot (pmol/mL*s), and SA is the surface area of the Transwell® filter insert (cm²).

The apparent permeability coefficient for atenolol and Lucifer yellow was calculated using eq. 2:

$$P_{app} = \frac{dQ}{dt} \cdot \frac{1}{SA \cdot C_0}$$

where dQ/dt is the rate of compound appearance in the basolateral chamber (pmol/s) under sink conditions, SA is the surface area of the Transwell® filter insert (cm²), and C_0 is the dosing concentration of compound in the apical compartment.

CYP3A activity assessment. Following experimental treatment as described above, monolayers were washed three times with blank apical transport buffer (10 mM HEPES in Hank's balanced salt solution, pH 6.5) and maintained at 37°C until use. A stock solution of midazolam (3 mM) was diluted in apical transport buffer to make the dosing solution (final concentration 8 μM midazolam, 0.27% methanol). Blank transport buffer was then removed, and 0.3 mL of the dosing solution was added to the filter insert and 0.7 mL of the receiver solution (10 mM HEPES in Hank's balanced salt solution, pH 7.4, containing 0.27% methanol) was added to the basolateral compartment. For HSA experiments, 1 g/dL of HSA was included in the receiver solution and 1 g/dL of dextran (70 kDa) was included in the apical chamber as an osmotic control. Cells were incubated for 60 minutes at 37°C and the total volume from the apical and basolateral compartment were collected separately and stored at -80°C until analysis. Parent midazolam and 1-OH midazolam was quantified as described above, with additional MRM transitions monitored: m/z 342 > 168.1 for 1-OH midazolam and m/z 346 > 168 for 1-OH midazolam- d_4 . For both 1-OH midazolam and 1-OH midazolam- d_4 , dwell time was set to 100 ms and cell accelerator voltage was set to 7 V. Fragmentor and collision energy was set to 143 V and 40 eV for 1-OH midazolam and 153 V and 44 eV for 1-OH midazolam- d_4 . The 4-OH midazolam metabolite was not monitored during these experiments, as the dose of midazolam used in these incubation would not lead to significant formation of the 4-OH midazolam metabolite (Fisher et al., 1999a).

Total protein determination for CYP3A activity normalization. As part of the assessment of CYP3A activity in primary enterocytes, LS180 cells, and Caco-2 cells, cells were washed three times with ice-cold DPBS⁺⁺. After the final wash, DPBS⁺⁺ was aspirated and 150 μL of 1M sodium hydroxide was added to the apical chamber of each Transwell to lyse the cells at room

temperature for 1 hour. While cells were incubating with sodium hydroxide, BCA standards (catalog no. 23208, Thermo Scientific, MA) were added to a 96-well plate and kept at 4°C until cell lyses was complete. After the hour incubation, 150 μ L of 1M HCl was added to each Transwell insert to neutralize the sodium hydroxide. The neutralized cell lysate solution (25 μ L) was added to the 96-well plate containing standards. BCA working reagent was prepared and 200 μ L was added to each well containing BCA standards or cell lysate. The plate was then incubated at 37°C for 30 minutes and then read on a Tecan SPARK multimode plate reader (Tecan Group Ltd., Switzerland), measuring an absorbance of 562 nm. The protein content of enteroid monolayers used for the CYP3A activity comparison experiment (i.e., monolayers of primary enterocytes, LS180, Caco-2 and differentiated enteroids) was not measured. As an alternative for activity normalization, we used the total protein content measured as described above in 208 different enteroid monolayers cultured under identical conditions; the coefficient of variation of that mean protein content (0.104 mg) was 16%.

Midazolam first-pass extraction ratio calculation. The midazolam first pass extraction ratio (ER) to assess CYP3A activity was calculated using eq. 3 (Fisher et al., 1999b):

$$ER = \frac{\Sigma(1 - OH MDZ)}{\Sigma(1 - OH MDZ) + MDZ_{Basolateral}}$$

where $\Sigma(1-OH MDZ)$ is the amount of 1-OH midazolam measured in both the apical and basolateral compartments (pmol) and $MDZ_{Basolateral}$ is the amount of unchanged midazolam measured in the basolateral compartment. The impact of CYP3A5 expression on total activity was not assessed in this paper – only one donor (donor 3) was heterozygous for the *CYP3A5*1* allele, and there was no obvious difference in catalytic activity between this donor and others.

P-gp activity assay. Cell monolayers were washed three times with blank transport buffer (10 mM HEPES in Hank's balanced salt solution, pH 7.4) and maintained at 37°C until use. For the basal and rifampin-induced conditions, stock solutions of the test compound (digoxin, 10 mM in DMSO) was diluted in donor transport buffer (pH 7.4) to make the final dosing solution (final concentrations of digoxin was 10 μ M, 0.1% DMSO). For the verapamil-inhibited condition, stock solutions of digoxin and verapamil (both 10 mM in DMSO) were diluted in donor transport buffer (pH 7.4) to make the final dosing solutions (final concentration of both digoxin and verapamil were 10 μ M, 0.2% DMSO). For each condition, a matched vehicle control containing the same %DMSO was run in parallel.

For the apical dosing conditions, 0.3 mL of the dosing transport buffers prepared above were added to the filter insert and 0.72 mL of transport buffer (pH 7.4) containing a matched amount of DMSO (v/v) was added to the basolateral compartment. For the basolateral dosing conditions, 0.7 mL of the dosing transport buffers prepared above were added to the basolateral compartment and 0.32 mL of transport buffer (pH 7.4) containing a matched amount of DMSO (v/v) was added to the filter insert. Cells were incubated for 30 minutes at 37°C and the total volume from all compartments were collected separately and stored at -80°C until analysis.

Digoxin was measured using liquid chromatography coupled with tandem mass spectrometry on an Agilent 6410 QQQ equipped with a UPLC 1290 system. After thawing and vortexing, 50 μ L of the receiver samples and 50 μ L of diluted donor samples (diluted 25-fold in blank transport buffer) were mixed with 20 μ L internal standard (3.75 ng/mL in methanol) and 30 μ L of methanol. Samples were then centrifuged at 20,800g for 10 minutes at 4°C, and 75 μ L of the supernatant was analyzed by LC/MS-MS. Chromatographic separation was achieved following injections of 10 μ L of sample using a Zorbax RX-C8 narrow bore, 5 μ m, 2.1 x 150 mm column

using 10 mM ammonium acetate, 1 mM ammonium chloride in water (A) and methanol (B) as mobile phase. The flow rate was 0.25 mL/min with a gradient as follows: 65% B for 1 minute, then increased to 100% linearly over 3 minutes, held at 100% for 3 minutes, and then equilibrated back to 65% for 2 minutes. The following SIM was monitored: m/z 815.5 for digoxin-chloride adduct, and m/z 818.5 for digoxin- d_3 -chloride adduct in negative mode. For both compounds, dwell time was set to 100 ms, cell accelerator voltage was set to 7 V, and fragmentor was set to 200 V. Results are presented as the peak area ratio of the analyte (digoxin) to internal standard (digoxin- d_3).

Efflux ratio calculation. The efflux ratio of digoxin was calculated using eq. 3:

$$ER = \frac{P_{app,B \rightarrow A}}{P_{app,A \rightarrow B}}$$

Where P_{app} values for the basolateral and apical dosing conditions were calculated as described in equation 2.

Statistical analysis. Prior to making comparisons, genes with very low expression levels were excluded, based on a mean log counts/million (logCPM) > 0 , which reduced the number of genes from just over 70,000 to 13,728 genes. Normalization factors were estimated using the trimmed-mean of M-values (TMM) method (Robinson and Oshlack, 2010), and then comparisons were made between differentiated and undifferentiated cells using a quasi-likelihood F-test (Lun et al., 2016), with a blocking factor to control for sample donor. The analysis was performed using the Bioconductor edgeR package (Robinson et al., 2010). To restrict to those genes with a large change in expression, an additional 20%-fold change criterion was included (e.g., the null hypothesis was specified as $H_0: |\beta| < 1.2$), using the treat function (McCarthy and Smyth, 2009).

Differentially expressed genes were selected using a false discovery rate (FDR) <0.05 (Benjamini and Hochberg, 1995).

Statistical significance ($\alpha = 0.05$) for the permeability and CYP3A metabolism studies was determined via linear mixed effect models. All statistical analyses were conducted using RStudio (R. Posit Software, PBC, Boston, MA)

RESULTS

Enteroid monolayer differentiation status and morphology. The effects of Wnt3A reduction on enteroid differentiation are shown in Supplemental Figure 1 and Figure 1. Numerous genes specific to various pathways, such as intestinal absorption, mucous secretion, cell proliferation, and xenobiotic metabolism/transport phenomena, are differentially expressed between undifferentiated spheroids and enteroid monolayers grown for 21 days in culture. mRNA expression of several of these genes, shown as Log₂CPM, is depicted in Figure 1a, where there was a decrease in mRNA abundance of cell proliferation genes, PCNA and MKI67, and an increase in enterocyte and goblet cell associated gene transcripts, sucrase isomaltase and MUC13, respectively. Interestingly, mRNA coding the stem cell marker, LGR5, did not change following differentiation, although there was significant inter-donor variability. Follow-up ICC experiments demonstrated the presence of a small population of proliferating cells as shown by the nuclear stain of a prototypical proliferation marker, Ki67 (Figure 1b). As expected, ICC experiments confirmed the absence of an enterocyte marker, villin, after 1 day in culture (Figure 1c) and its presence after 7 days in culture (Figure 1d). Enteroid monolayers cultured for 21 days in differentiation media demonstrate a mixed-cobblestone morphology under brightfield microscopy and an undulating-like surface as seen in orthogonal images (Figure 2a and 2b). The

presence and proper localization of prototypical apical- and basolateral-associated proteins, ZO-3 and MRP3 respectively, was confirmed via ICC experiments (Figure 2c).

Cell monolayer barrier integrity. TEER values for differentiated enteroid monolayers from three donors were measured during a 21-day culture period. As shown in Figure 3a, TEER values for the differentiated enteroid monolayers rose steadily, achieving an apparent plateau by day 11-15 for two donors; values ranged from approximately 200 to 600 $\Omega\cdot\text{cm}^2$. In contrast, TEER values for a representative undifferentiated organoid monolayer were substantially lower throughout the entire culture period, reaching a maximum of approximately 40 $\Omega\cdot\text{cm}^2$. A follow-up study assessing the stability of TEER values of a differentiated enteroid monolayer from a single representative donor over 42 days is shown in Figure 3b. The TEER values for this donor had a similar trajectory as the 21-day experiment, plateauing at approximately 400 $\Omega\cdot\text{cm}^2$ after 21-days in culture and remaining there through day 42.

A functional 21-day permeability study was conducted with differentiated enteroid monolayers from three donors utilizing the paracellular marker probe substrates, atenolol and Lucifer yellow, and the highly permeable transcellular marker probe, midazolam. As shown in Figure 3c, the apparent permeability (P_{app}) values for midazolam were approximately 17×10^{-6} cm/s on days 7 and 21. In contrast, the paracellular transport probe compounds atenolol and Lucifer yellow demonstrated P_{app} values comparable to the midazolam values on day 7 in culture but decreased to approximately 5×10^{-6} cm/s by day 21 in culture.

Barrier integrity was also assessed via ICC imaging of tight junction proteins (Figure 4a-4c). Occludin, ZO-1, and ZO-3 all demonstrated organized localization at the cell-cell boundaries in monolayers cultured for 21 days and ZO-3 in monolayers cultured for 42 days (Figure 4d).

RNA expression of various DMET genes. The abundances in undifferentiated spheroids and differentiated monolayers grown for 21 days of mRNA encoded by various DMET genes was compared (Figure 5a and 5b). The expression of most DMET genes increased following differentiation, including both phase I (CYP3A4) and phase II enzymes (UGT1A1, SULT2B1) and both SLC (SLC51A, OST α/β) and ABC (ABCB1, P-gp) transporters.

Midazolam extraction ratios in enteroid monolayers. A comparison of basal CYP3A activity, expressed as 1-OH midazolam formed per milligram of total protein, for enteroid monolayers grown for 7 and 21 days to primary enterocytes, LS180, and Caco-2 cells is shown in figure 6A. These results demonstrate that differentiated enteroid monolayers have greater CYP3A activity than LS180 and Caco-2 cells, and enteroid monolayers grown for 21 days have greater CYP3A activity than primary enterocytes. A follow up study of CYP3A activity in enteroid monolayers cultured for 7 and 21 days was assessed by calculation of first-pass (A>B) midazolam extraction ratios, in basal, induced, and inhibited states (Figure 6B). Basal extraction ratios ranged from 4-15% at day 7 in culture and increased to 12-30% by day 21 in culture. Addition of the prototypical vitamin D receptor (VDR) ligand and CYP3A4 inducer, 1 α ,25(OH) $_2$ vitamin D $_3$, increased the midazolam extraction ratios at culture day 7 and day 21 to approximately 13-28% and 25-50%, respectively. The addition of a known mechanism-based inactivator of intestinal CYP3A4, 6',7'-dihydroxybergamottin, decreased midazolam extraction ratios at day 7 and day 21 in culture to approximately 0-3% and 0-4% of basal control. An additional study assessing the enteroid monolayer midazolam extraction ratio under basal and CYP3A-induced conditions after 42 days in culture is shown in Figure 6C; values for basal and vitamin D-treated monolayers ranged from 6-42% and 19-52%, respectively.

Pharmacokinetic theory predicts that the presence of albumin in the vascular compartment of mucosal villi can affect both the permeability and metabolic extraction of orally administered CYP3A substrates, depending on albumin-drug binding affinity and the site of the rate-determining step in transcellular flux (Fisher et al., 1999a). The effect of HSA addition to the differentiated enteroid monolayer basolateral (i.e., vascular) compartment on apically dosed midazolam extraction ratios is shown in Table 1. The addition of HSA resulted in approximately a 25% decrease in midazolam extraction ratio for donor monolayers. The decrease in midazolam extraction ratio was accompanied by an increase in midazolam monolayer permeability; P_{app} was increased approximately 2-fold compared to no HSA control. Of note, the rate of formation of 1'-hydroxymidazolam during the same 1-hr assessment period remained unchanged.

DISCUSSION

The development of an intestinal enterocyte monolayer model to predict oral drug disposition is of particular interest to the field of pharmaceutical science. The intestinal organoid is an emerging tool that addresses this interest, however, current reports utilizing intestinal organoids describe complete Wnt3A-removal to achieve terminal organoid differentiation, imparting limited viability of roughly one week and continuing dynamic changes in DMET functions (Michiba et al., 2022). Results presented in this article demonstrate that the use of a proprietary media formulation which promotes differentiation, provided by Intesticult, can elicit enterocyte differentiation, including functional barrier integrity and CYP3A enzyme activity, and that differentiation and cell viability is stable for an extended period of time (3-6 weeks). Under these conditions, enteroid monolayers showed a decline in mRNA for markers of cell proliferation (PCNA and MKI67) and an increase for cell type-specific markers for enterocytes and goblet cells (sucrase isomaltase and MUC13, respectively), compared to undifferentiated intestinal

spheroids. Pathway analysis of the RNA-Seq data supports these selected observations, as genes related to cell proliferation, intestinal absorptive/secretory processes, and xenobiotic metabolism/transport processes were differentially expressed between undifferentiated spheroids and enteroid monolayers. Interestingly, mRNA abundance of the stem cell marker, LGR5, in undifferentiated spheroids and differentiated enteroid monolayers was not statistically different (although a highly variable decreased trend apparent), suggesting that these monolayers contain a population of dividing cells that confers a self-renewing phenotype. Corroborating this interpretation was the identification of proliferating cells in the enteroid monolayer, as demonstrated by sporadic nuclear localization of Ki67 protein. Collectively, our results suggest that enteroid monolayers differentiated in this proprietary medium are amenable to long-term studies of the multiple processes affecting oral intestinal drug bioavailability.

Enteroid monolayers cultured for 21 days exhibited a mixed-cobblestone morphology under brightfield microscopy – a lack of uniformity in the monolayer is expected from a culture of a mixed population of cells, such as those found in the intestinal villi that are generated by the same crypt stem cell precursor (Barker et al., 2007). Interestingly, orthogonal imaging of DAPI stained nuclei in these monolayers demonstrated spontaneous formation of an undulating-like surface. Though not complete formation of a crypt-villus axis as seen *in vivo*, this observation suggests that the enteroid monolayers are self-organizing into an anatomically relevant structure. Monolayer morphology was further assessed by confirming the proper localization of prototypical apical and basolateral membrane-associated proteins, ZO-3 and MRP3, respectively, indicative of monolayer polarization.

We next explored the barrier function of intestinal monolayers. Measuring TEER allowed us to assess the maturation of the epithelial barrier during the entire study period. Results showed

a time-dependent maturation of barrier function (10-14 days), but also relative stability in that function between 14-42 days. Permeability studies utilizing paracellular transport probe substrates corroborated TEER measurements. Importantly, the permeability of Lucifer yellow and atenolol were comparable to that of the highly permeable control, midazolam, on day 7 in culture, but were roughly 3-fold lower by day 21 in culture, demonstrating development of a functional barrier by this time. It should be noted that the P_{app} values calculated in this experiment are likely overestimated, given that the surface area used for these calculations was that of the Transwell® membrane but the true surface area of the cells was likely greater due to the undulations seen by microscopy and the potential presence of microvilli. ICC results confirmed the presence of inter-cellular tight junction proteins in enteroid monolayers, which is expected for a functioning paracellular barrier. Collectively, our study results suggest that enteroid monolayers differentiated using a proprietary differentiation medium maintain barrier integrity over an extended period and are amenable to repeated measurements of drug absorption across the intestinal mucosa under different experimental conditions.

As expected, the abundances of important DMET transcripts were increased in enteroid monolayers cultured for 21 days, compared to undifferentiated intestinal spheroids. Strikingly, the expression of both CYP3A4 and ABCB1 (P-glycoprotein) were among the most highly upregulated genes following differentiation, each with an approximately 60-fold mean increase in expression, although with high inter-donor variability. Following these findings, we characterized CYP3A activity in differentiated enteroid monolayers. We first compared the midazolam 1'-hydroxylation activity of enteroid monolayers to that of primary enterocytes, LS180 cells and Caco-2 cells cultured in the Transwell system under similar conditions. Results demonstrated superior basal activity from the enteroid monolayer cultured for 21 days, compared

to the other conventionally used intestinal cell models. In subsequent experiments, we found that enteroid monolayers were capable of first pass midazolam metabolic extraction (19-52%) that was comparable to that found *in vivo* (18-59%) (Paine et al., 1996), and the extraction was inducible and susceptible to mechanism-based inhibition. The strong agreement between the *in vivo* report and our *in vitro* data highlights the biochemical relevance of enteroid monolayers as a tool to predict oral first-pass drug metabolism. Indeed, our limited results from enteroid monolayers grown for 42 days in culture suggest stable metabolic function for at least 6 weeks, presumably as a consequence of self-replication during the treatment period, as would occur *in vivo*.

To further assess the utility of the enteroid monolayer model, we investigated a more physiologically relevant situation where binding proteins (HSA) are present in the basolateral chamber that might impact both midazolam permeability and extraction ratio. As hypothesized, basolateral HSA increased midazolam permeability by approximately 2-fold. Midazolam exhibits high protein binding *in vivo* of around 97%, so the addition of abluminal HSA would produce a lower concentration of unbound midazolam in the basolateral chamber than in the absence of HSA, which could facilitate passive diffusion across the basolateral membrane by maintaining a high unbound midazolam concentration gradient. The increase in cell permeability was accompanied by a modest decrease in midazolam extraction ratio of about 25%, but no change in midazolam 1'-hydroxylation rate. This combination of results suggests that midazolam cell efflux across the basolateral membrane is rate-limiting, compared to uptake into the cell from the apical compartment. An equilibrium between apical and intracellular compartments is likely rapidly achieved and is unaffected by midazolam binding to basolateral HSA. The reduction in first-pass extraction is achieved by an increase in basolateral cell permeability and not a decrease

in metabolism. These findings and conclusions may be applicable to other highly bound BCS Class 1 drugs.

A limitation of this study is the number of stem cell donors (n=3) utilized for experimentation. Future studies should look at a larger pool of donors to ascertain potential sources of interindividual variability in oral drug absorption and/or metabolism. An additional limitation is that only CYP3A activity was assessed. While it is well-established that CYP3A4 is the most abundant cytochrome P450 enzyme in the small intestine, other enzymes including both phase I and phase II are also present and should be assessed in future studies; including CYP2C9, CYP2C19, CES2, and UGT1A isoforms. Similarly, the activity of various efflux and uptake transporters, such as P-gp (ABCB1), PEPT1, OATP2B1, and various organic cation transporters, was not rigorously assessed in this work – future studies need to address this gap as transporters play an important role in modulating oral drug absorption and are a potential source of drug-drug/natural product-drug interactions. In this regard, pilot experiment investigating P-gp function using digoxin as a probe substrate in enteroid monolayers grown for 7 days suggests that functional P-gp is present and that efflux activity increases in the presence of an inducer (rifampin) and decreases in the presence of an inhibitor (verapamil) (Supplemental Figure 2). While encouraging, this study needs to be repeated across more donors and for enteroid monolayers grown for 21 days before firmer conclusions can be drawn. Moreover, this study did not assess changes in DMET mRNA abundance following treatment with $1\alpha,25(\text{OH})_2$ vitamin D₃. While the CYP3A activity results suggest CYP3A transcription was increased, assessing the impact of $1\alpha,25(\text{OH})_2$ vitamin D₃ on other DMET transcripts would help bolster the claim that enteroid monolayers respond appropriately to this stimulus. Additionally, this study did not assess differences in enteroid viability and function when enteroids were differentiated using a

proprietary medium versus a medium that is completely devoid of Wnt3A. Furthermore, this publication did not fully investigate the differentiation stability between day 21 and day 42 enteroids – CYP3A activity data suggests stability, but additional metrics are needed to support this claim.

In summary, results from experiments detailed in this report support the use of human crypt stem cell derived enteroid monolayers as an *in vitro* model to study oral drug disposition. Cell culture with a proprietary differentiation medium imparted an extended viability that is not present for enteroid monolayers differentiated in a medium that is devoid of Wnt3A. Long term-cultured enteroids could have unique utility, compared to other *in vitro* models, for studying complex kinetic phenomena such as the time-course of perturbations in enzyme or transporter function/expression, as well as the interplay of intestinal transport and metabolism processes, such as P-gp and CYP3A (Benet et al., 1996), and *in vitro-in vivo* PBPK modeling. Moreover, this model might be more amenable for studying intestinal drug accumulation kinetics in the treatment of intestinal diseases, xenobiotic intestinal toxicity and the impact of chronic conditions such as microbial or disease-induced inflammation. Additional work is needed to explore these applications.

ACKNOWLEDGMENTS

We thank Dr. Dale Hailey for his assistance and expertise in confocal microscopy. We thank Dr. Laura Shireman, Linda Risler, and Calder Brauchla for their assistance and expertise in quantitative mass spectroscopy analysis. We thank Dr. Leila Zelnick for her help with statistical analysis. The analysis of the RNA-sequencing data for this study was supported by the University of Washington Interdisciplinary Center for Exposures, Diseases, Genomics, and Environment.

AUTHOR CONTRIBUTIONS

Participated in research design: Arian, O'Mahony, Donowitz, Kelly, and Thummel.

Conducted experiments: Arian and O'Mahony.

Contributed new reagents or analytical tools: Donowitz.

Performed Data Analysis: Arian, O'Mahony, Macdonald, Bammler.

Wrote or contributed to the writing of the manuscript: Arian, O'Mahony, Macdonald, Bammler, Donowitz, Kelly, and Thummel.

References

- Andrews S (2010) Babraham Bioinformatics - FastQC a quality control tool for high throughput sequence data, <https://www.bioinformatics.babraham.ac.uk/projects/fastqc/>.
- Anoshchenko O, Storelli F, and Unadkat JD (2021) Successful Prediction of Human Fetal Exposure to P-Glycoprotein Substrate Drugs Using the Proteomics-Informed Relative Expression Factor Approach and PBPK Modeling and Simulation. *Drug Metab Dispos* **49**:919-928.
- Arian CM, Imaoka T, Yang J, Kelly EJ, and Thummel KE (2022) Gutsy science: In vitro systems of the human intestine to model oral drug disposition. *Pharmacol Ther* **230**:107962.
- Barker N, van Es JH, Kuipers J, Kujala P, van den Born M, Cozijnsen M, Haegebarth A, Korving J, Begthel H, Peters PJ, and Clevers H (2007) Identification of stem cells in small intestine and colon by marker gene *Lgr5*. *Nature* **449**:1003-1007.
- Benet LZ, Wu C-Y, Hebert MF, and Wachter VJ (1996) Intestinal drug metabolism and antitransport processes: A potential paradigm shift in oral drug delivery. *Journal of Controlled Release* **39**:139-143.
- Benjamini Y and Hochberg Y (1995) Controlling the False Discovery Rate: A Practical and Powerful Approach to Multiple Testing. *Journal of the Royal Statistical Society: Series B (Methodological)* **57**:289-300.
- Fisher JM, Wrighton SA, Calamia JC, Shen DD, Kunze KL, and Thummel KE (1999a) Midazolam metabolism by modified Caco-2 monolayers: effects of extracellular protein binding. *J Pharmacol Exp Ther* **289**:1143-1150.
- Fisher JM, Wrighton SA, Watkins PB, Schmiedlin-Ren P, Calamia JC, Shen DD, Kunze KL, and Thummel KE (1999b) First-pass midazolam metabolism catalyzed by 1 α ,25-

- dihydroxy vitamin D3-modified Caco-2 cell monolayers. *J Pharmacol Exp Ther* **289**:1134-1142.
- Foulke-Abel J, In J, Yin J, Zachos NC, Kovbasnjuk O, Estes MK, de Jonge H, and Donowitz M (2016) Human Enteroids as a Model of Upper Small Intestinal Ion Transport Physiology and Pathophysiology. *Gastroenterology* **150**:638-649 e638.
- In JG, Foulke-Abel J, Estes MK, Zachos NC, Kovbasnjuk O, and Donowitz M (2016) Human mini-guts: new insights into intestinal physiology and host-pathogen interactions. *Nat Rev Gastroenterol Hepatol* **13**:633-642.
- Kasendra M, Luc R, Yin J, Manatakis DV, Kulkarni G, Lucchesi C, Sliz J, Apostolou A, Sunuwar L, Obrugewitch J, Jang KJ, Hamilton GA, Donowitz M, and Karalis K (2020) Duodenum Intestine-Chip for preclinical drug assessment in a human relevant model. *Elife* **9**.
- Kim D, Paggi JM, Park C, Bennett C, and Salzberg SL (2019) Graph-based genome alignment and genotyping with HISAT2 and HISAT-genotype. *Nat Biotechnol* **37**:907-915.
- Liao Y, Smyth GK, and Shi W (2019) The R package Rsubread is easier, faster, cheaper and better for alignment and quantification of RNA sequencing reads. *Nucleic Acids Res* **47**:e47.
- Lun AT, Chen Y, and Smyth GK (2016) It's DE-licious: A Recipe for Differential Expression Analyses of RNA-seq Experiments Using Quasi-Likelihood Methods in edgeR. *Methods Mol Biol* **1418**:391-416.
- McCarthy DJ and Smyth GK (2009) Testing significance relative to a fold-change threshold is a TREAT. *Bioinformatics* **25**:765-771.
- Michiba K, Maeda K, Shimomura O, Miyazaki Y, Hashimoto S, Oda T, and Kusuhara H (2022) Usefulness of Human Jejunal Spheroid-Derived Differentiated Intestinal Epithelial Cells

- for the Prediction of Intestinal Drug Absorption in Humans. *Drug Metab Dispos* **50**:204-213.
- Paine MF, Shen DD, Kunze KL, Perkins JD, Marsh CL, McVicar JP, Barr DM, Gillies BS, and Thummel KE (1996) First-pass metabolism of midazolam by the human intestine. *Clin Pharmacol Ther* **60**:14-24.
- Robinson MD, McCarthy DJ, and Smyth GK (2010) edgeR: a Bioconductor package for differential expression analysis of digital gene expression data. *Bioinformatics* **26**:139-140.
- Robinson MD and Oshlack A (2010) A scaling normalization method for differential expression analysis of RNA-seq data. *Genome Biol* **11**:R25.
- Rossi G, Manfrin A, and Lutolf MP (2018) Progress and potential in organoid research. *Nat Rev Genet* **19**:671-687.
- Rowland M, Tozer TN, and Rowland M (2009) *Pharmacokinetics and pharmacodynamics : concepts and clinical applications*. Lippincott William & Wilkins, Philadelphia.
- Sato T, Stange DE, Ferrante M, Vries RGJ, van Es JH, van den Brink S, van Houdt WJ, Pronk A, van Gorp J, Siersema PD, and Clevers H (2011) Long-term Expansion of Epithelial Organoids From Human Colon, Adenoma, Adenocarcinoma, and Barrett's Epithelium. *Gastroenterology* **141**:1762-1772.
- Vernetti L, Gough A, Baetz N, Blutt S, Broughman JR, Brown JA, Foulke-Abel J, Hasan N, In J, Kelly E, Kovbasnjuk O, Repper J, Senutovitch N, Stabb J, Yeung C, Zachos NC, Donowitz M, Estes M, Himmelfarb J, Truskey G, Wikswa JP, and Taylor DL (2017) Functional Coupling of Human Microphysiology Systems: Intestine, Liver, Kidney Proximal Tubule, Blood-Brain Barrier and Skeletal Muscle. *Sci Rep* **7**:42296.

Footnotes

Funding:

- This work was supported in part by funding from the National Institutes of Health/ National Institute of Diabetes and Digestive and Kidney Diseases (U54 AT008909, R01 DK116352, U01 DK10316, P30 DK089502), the UW Drug Metabolism and Transport in Systems Pharmacology Research, and National Center For Advancing Translational Sciences of the National Institutes of Health under Award Number TL1 TR002318, and the University of Washington Interdisciplinary Center for Exposures, Diseases, Genomics, and Environment funded by the National Institute of Environmental Health Sciences (NIEHS P30 ES007033).

Conflicts:

- No author has an actual or perceived conflict of interest with the contents of this article.

Data Availability:

- The RNA-seq data has been submitted to NCBI's GEO data base and is publicly accessible via accession number GSE253641.

Tables

Table 1. HSA impact on midazolam disposition. Effect of abluminal HSA on midazolam ER, permeability, and 1-OH midazolam formation for monolayers grown for 7 and 21 days is shown in Table 1. Data is represented as the mean and SD of three donors with three culture replicates each.

Day 7				Day 21			
(-)HSA	(+) HSA	(-)HSA vs (+)HSA		(-)HSA	(+) HSA	(-)HSA vs (+)HSA	
Mean (SD)	Mean (SD)	p-value		Mean (SD)	Mean (SD)	p-value	
Midazolam First-Pass Extraction Ratio (%)				Midazolam First-Pass Extraction Ratio (%)			
Basal	10.2 (5.4)	5.5 (3.8)	4.3×10^{-6}	Basal	20.6 (9.3)	15.3 (11.9)	0.0055
Vitamin D	20.0 (7.3)	13.7 (7.2)	1.2×10^{-4}	Vitamin D	35.0 (13.3)	26.6 (12.8)	8.0×10^{-5}
Midazolam Permeability (10^{-6} cm/s)				Midazolam Permeability (10^{-6} cm/s)			
Basal	11.3 (3.0)	23.3 (3.7)	2.7×10^{-8}	Basal	14.2 (1.6)	27.7 (9.1)	7.1×10^{-5}
Vitamin D	11.5 (2.3)	19.2 (2.8)	1.7×10^{-6}	Vitamin D	14.7 (4.2)	23.5 (5.0)	1.4×10^{-5}
1-OH Midazolam formed (pmol)				1-OH Midazolam formed (pmol)			
Basal	10.1 (6.5)	10.3 (7.5)	0.61	Basal	26.4 (15.5)	31.5 (22.3)	0.23
Vitamin D	22.1 (12.1)	23.5 (14.5)	0.43	Vitamin D	54.0 (24.4)	57.9 (29.3)	0.18

FIGURE LEGENDS

Figure 1. Enteroid differentiation status. Effect of differentiation on gene expression of differentiation markers for undifferentiated spheroids and enteroid monolayers grown for 21 days expressed as the logarithm of counts per million reads (LogCPM) (a). Data points correspond to gene expression of an individual culture replicate, data point shape corresponds to organoid donor. Data represents means and SD of all culture replicates from three donors. ICC results are shown in figures 1b-d. Enteroids display a small population of Ki67 positive cells (green) by day 21 in culture (b). Enteroids lack robust staining of the enterocyte marker, Villin (green), at day 1 of culture (c) but demonstrate robust staining by day 7 (d). All scale bars represent 100 μm . *** $P < 0.001$.

Figure 2. Enteroid morphology. Enteroid monolayers under brightfield microscopy display a mixed-cobblestone morphology (a). Orthogonal images of DAPI (blue) stained nuclei show enteroids have an undulating morphology (b). Staining for ZO-3 (green) and MRP3 (magenta) confirm proper localization of apical and basolateral membrane proteins, respectively (c). All images are from enteroid monolayers grown for 21 days. The ZO-3 image in (c) is the same image as the orthogonal image in figure 4b. Scale bar represents 100 μm .

Figure 3. Barrier integrity. Transepithelial electrical resistance (TEER) values over time for enteroid monolayers grown on Transwell® inserts for 21 days (a) and 42 days (b). Data represents means and SD for culture replicates ($n = 6$ for donor 1, $n = 9$ for donor 2 and donor 3, $n = 3$ for undifferentiated monolayers) for each donor. Permeability studies for cells grown on Transwell® inserts for 7 and 21 days are shown in figure c. Data represents means and SD for each donor with three culture replicates each. *** $P < 0.001$.

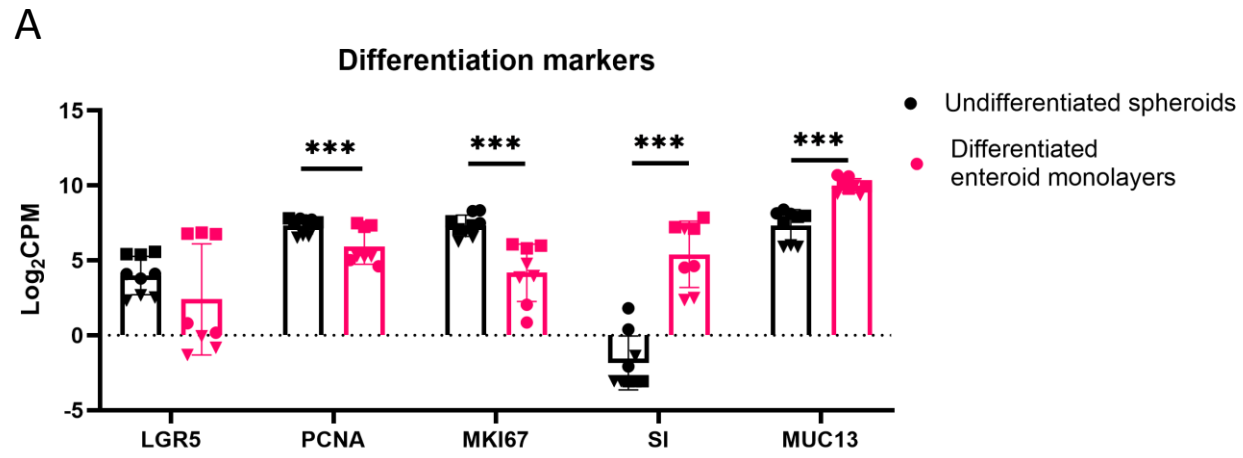
Figure 4. Tight junction proteins. ICC imaging of tight junction proteins, ZO-1 (green), ZO-3 (green), and Occludin (magenta), are shown in (a), (b), and (c), respectively, for enteroid monolayers grown for 21 days. Figure 4d shows ICC imaging of ZO-3 for enteroid monolayers grown for 42 days. Orthogonal images of each stain are shown below, where nuclei were counterstained with DAPI (blue). The orthogonal image of the ZO-3 stain in (b) is the same image shown in figure 2c. Scale bars represent 20 μm .

Figure 5. DMET RNA expression. The RNA expression of drug metabolizing enzymes (a) and transporters (b) for undifferentiated spheroids and enteroid monolayers grown for 21 days. Data points correspond to gene expression of an individual culture replicate, data point shape corresponds to organoid donor. Data represents means and SD of all culture replicates from three donors. * $P < 0.05$, *** $P < 0.001$.

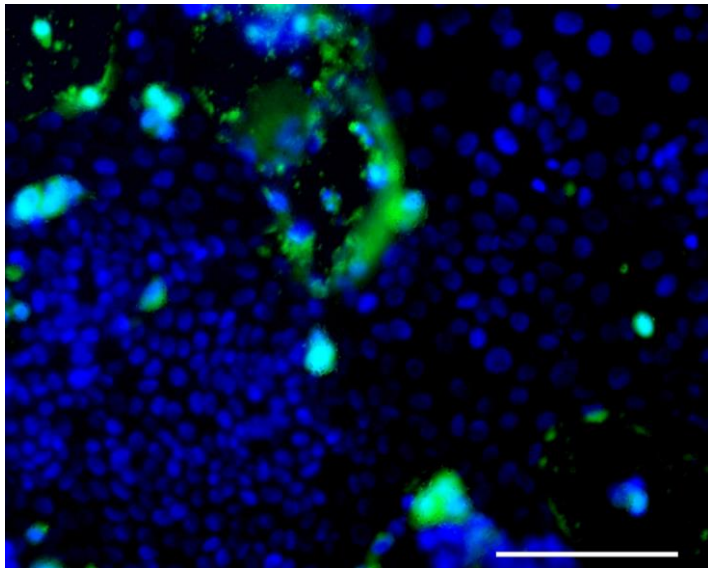
Figure 6. CYP3A activity. A comparison of CYP3A activity, expressed as 1-OH midazolam formed per milligram of total protein, for primary enterocytes from a single donor, LS180 cells, Caco-2 cells, and enteroid monolayers grown for 7 and 21 days is shown in (a). CYP3A activity results, expressed as midazolam metabolic first pass extraction ratios (ERs), for enteroid monolayers grown for 7 and 21 days under basal, 6',7'-dihydroxybergamottin, and vitamin D conditions are shown in (b), where the 6',7'-dihydroxybergamottin treatment was conducted with only 2 of the 3 available stem cell donors. Midazolam metabolic first pass extraction ratio (ER) for enteroid monolayers grown for 42 days is compared to the 7 and 21 day results in (c). For (a), primary enterocytes from a single donor, LS180, and Caco-2 data represent means and SD of three culture replicates from a single source. For the enteroid monolayers, data represents means and SD of three donors combined, containing three culture replicates each. For (b) and (c), data

represents means and SD for each donor with three culture replicates each. * $P < 0.05$, *** $P < 0.001$.

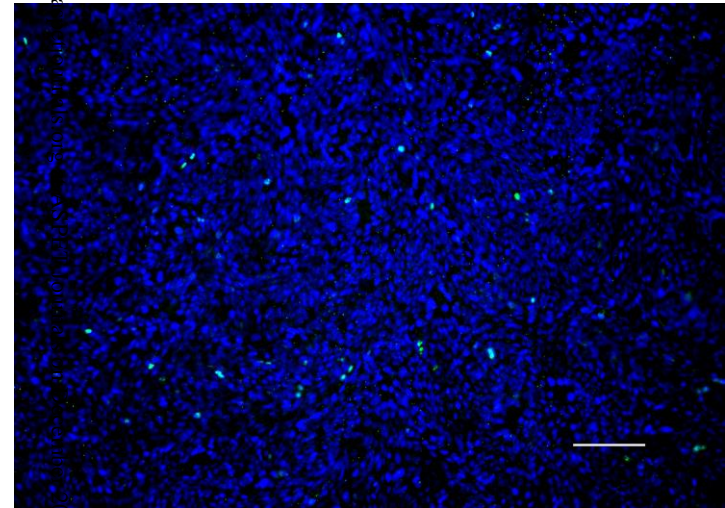
Figure 1



C



B



D

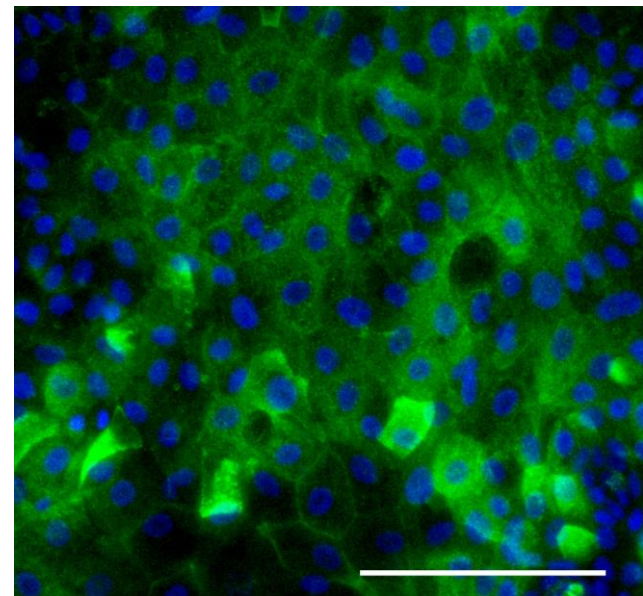
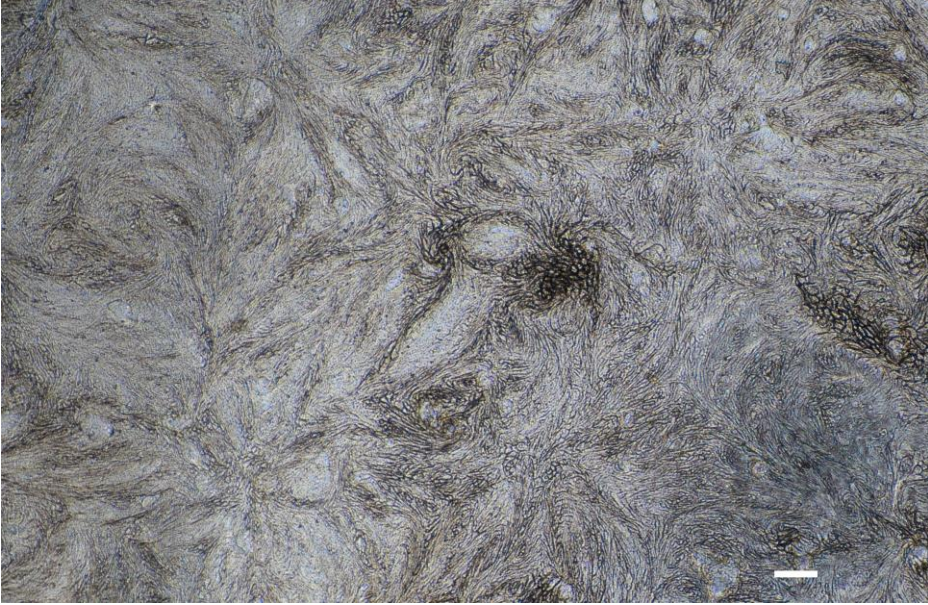
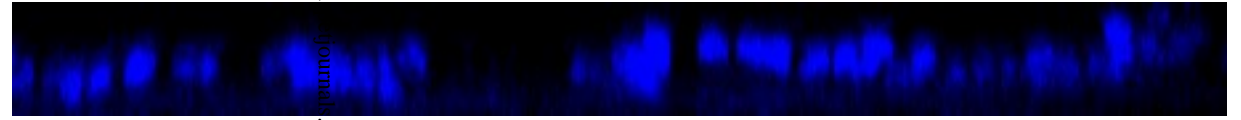


Figure 2

A

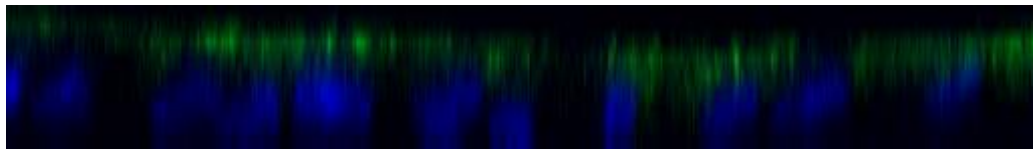


B



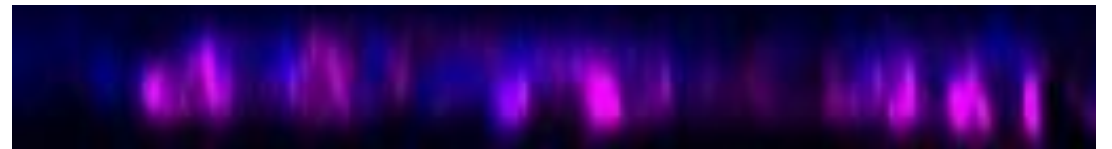
C

Apical



Basolateral

Apical



Basolateral

Figure 3

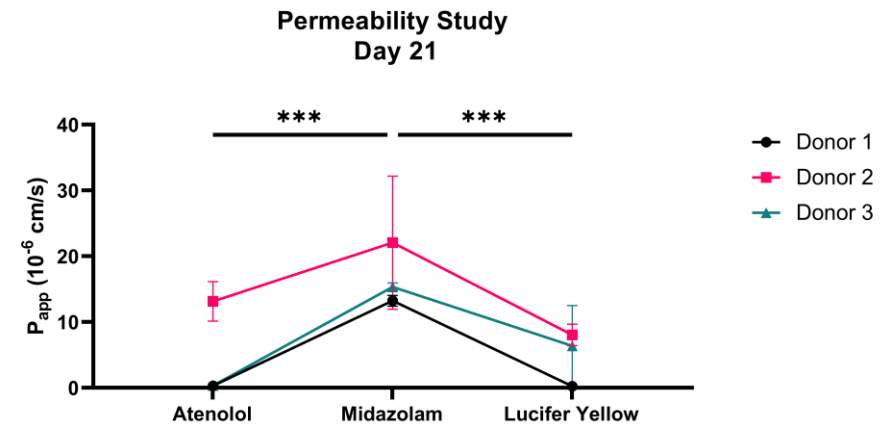
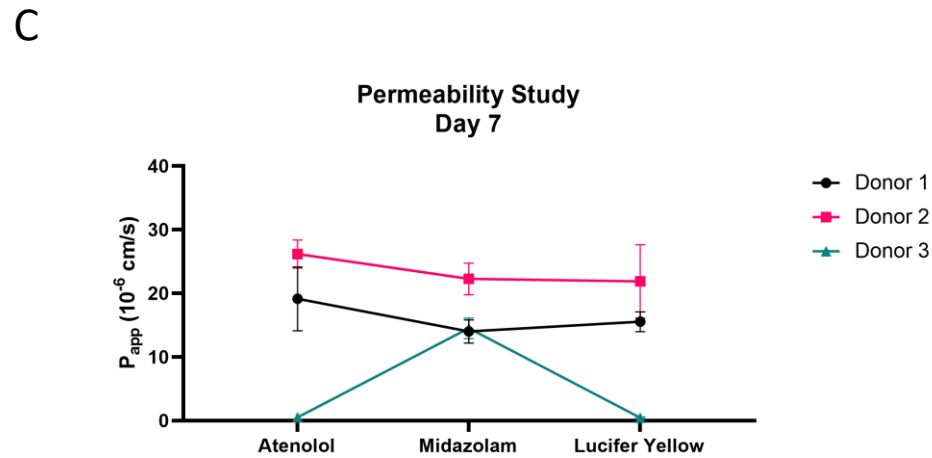
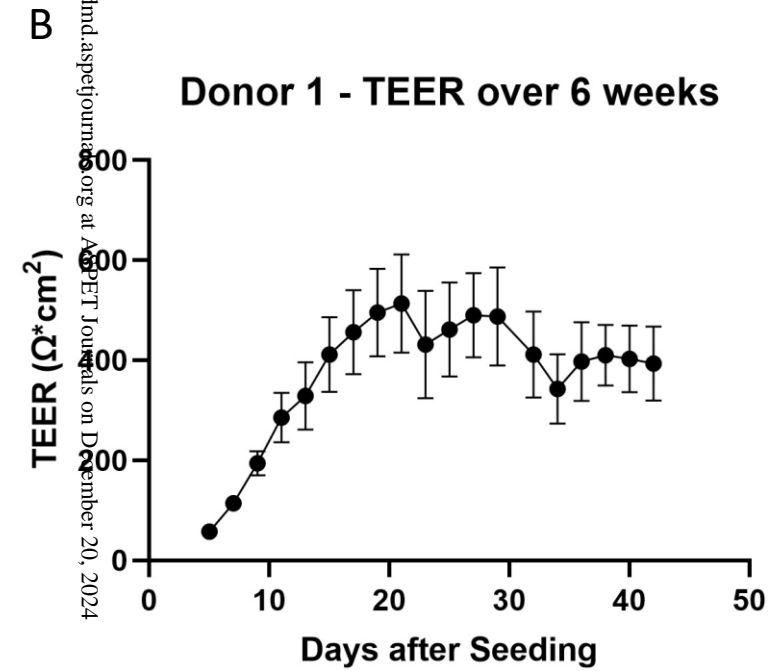
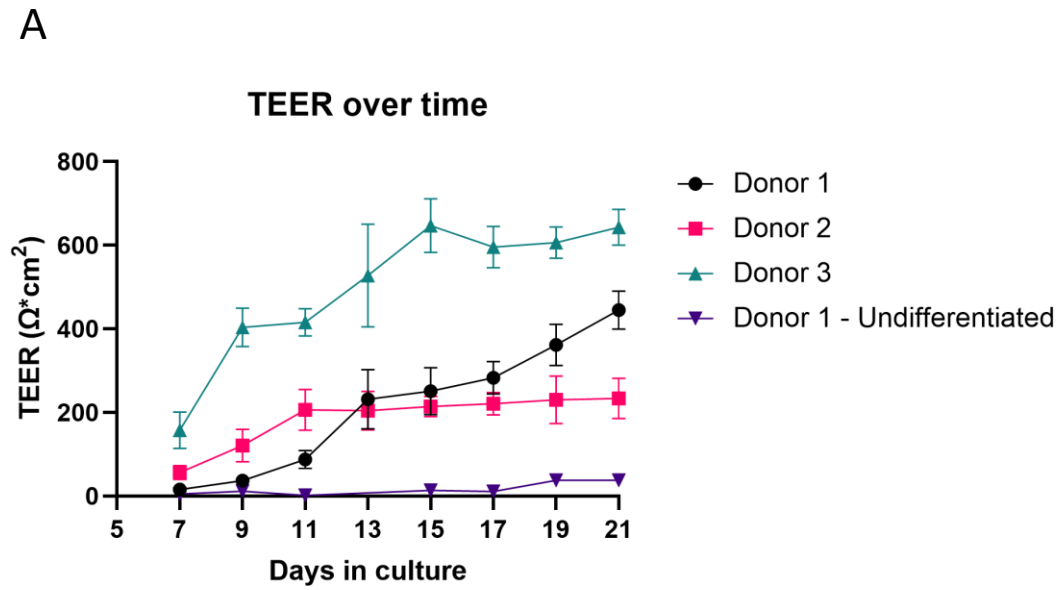
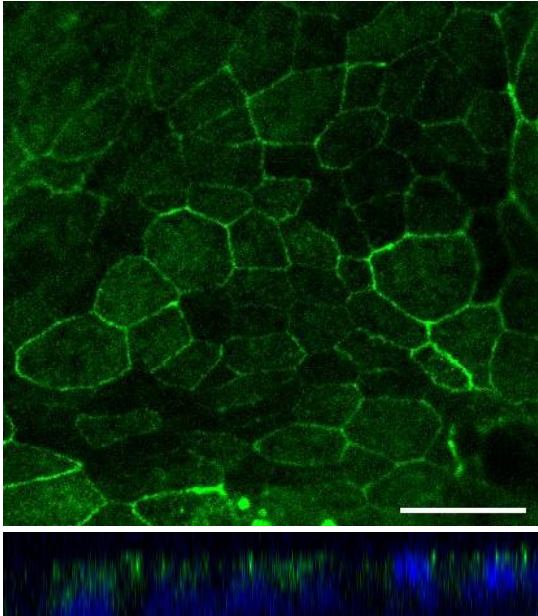
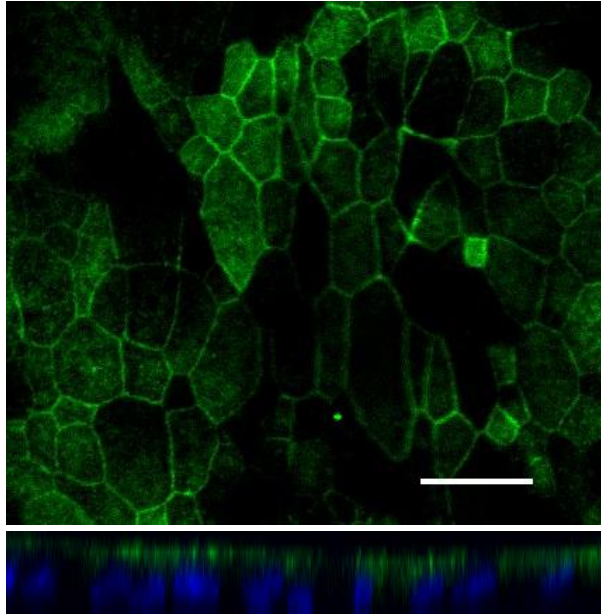


Figure 4

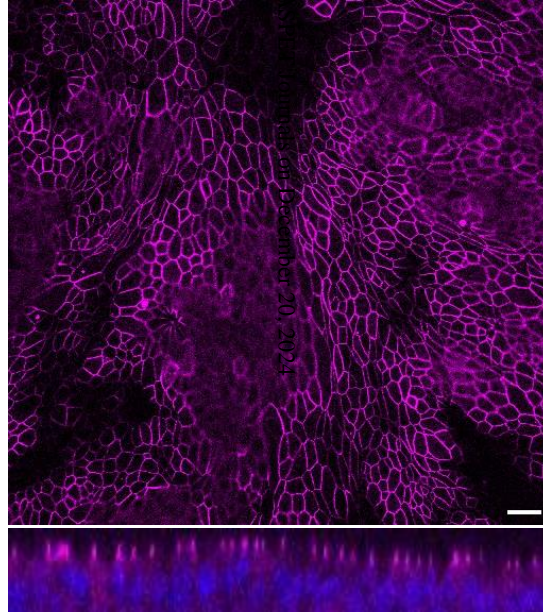
A



B



C



D

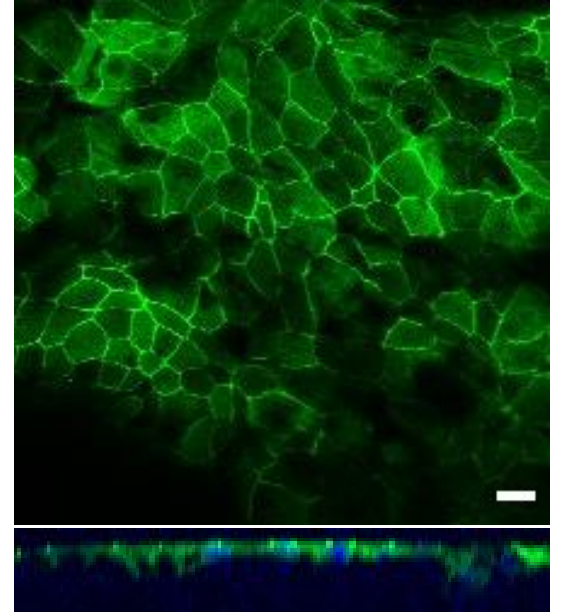
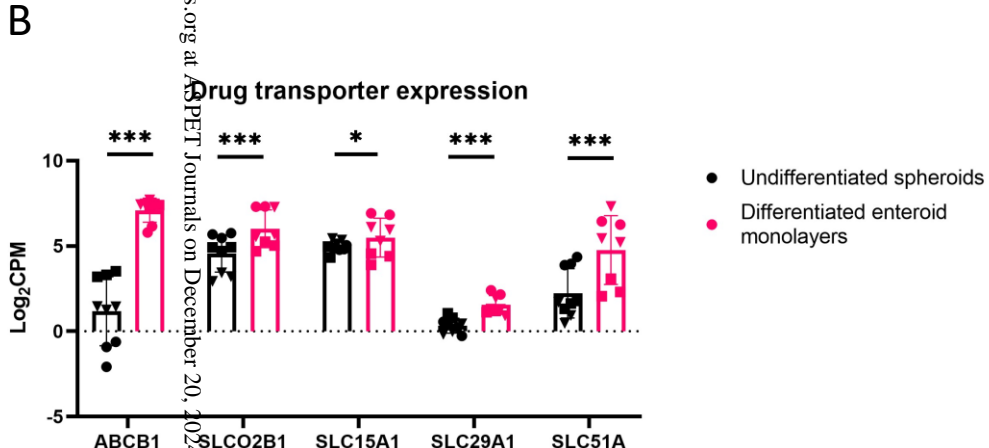
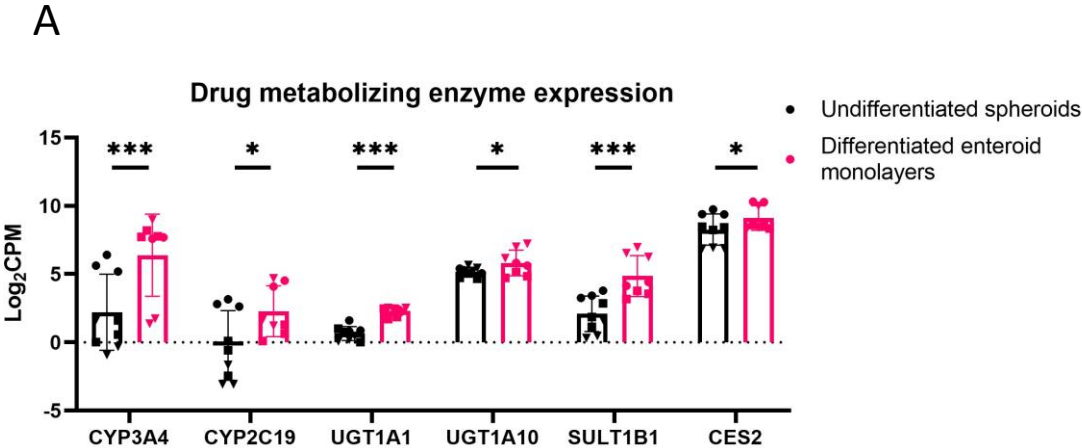
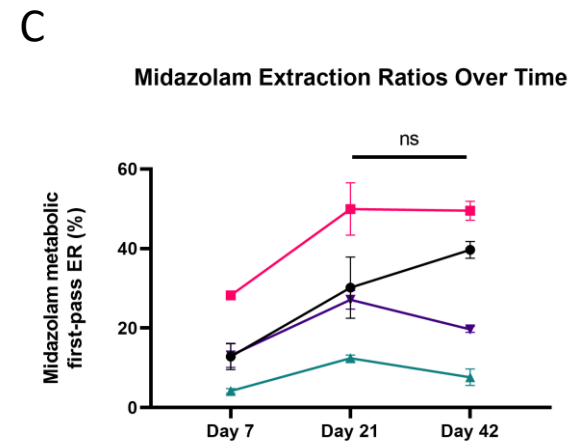
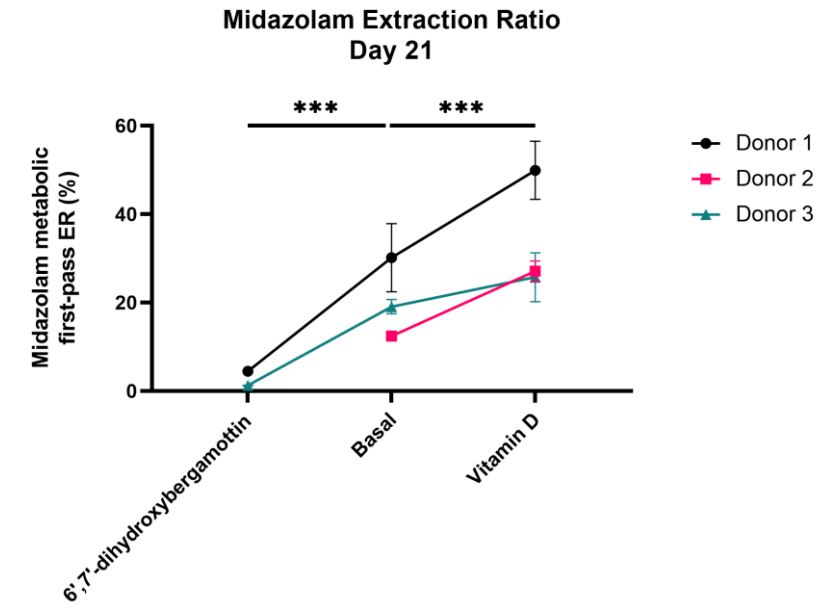
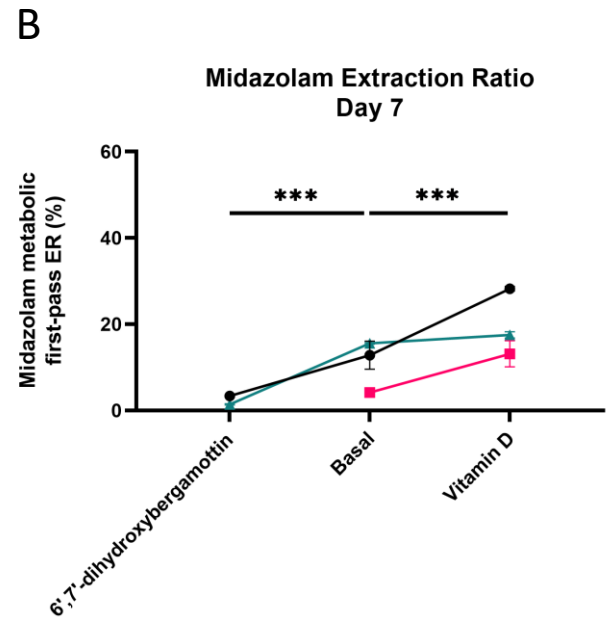
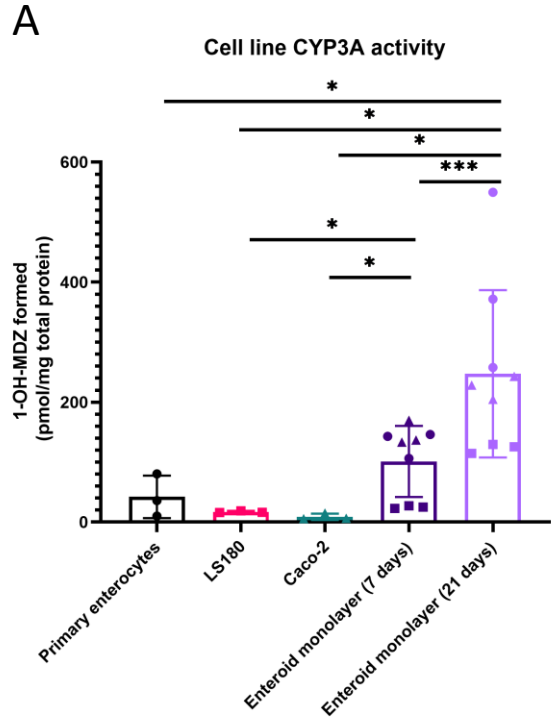


Figure 5



Downloaded from dmd.aspetjournal.org at ASPET Journals on December 20, 2024

Figure 6



Downloaded from dmd.aspetjournals.org at ASPET Journals on December 20, 2024